項目	周波数	送受挿入損失	焦点距離
単位	〔MHz〕	〔dB〕	〔mm〕
規格※	400	55 以上	0.29±0.03
測定値	326	48	0.31
	400	55	

表 1 振動子の特性

2. 新型トランスデューサへの取り組み

超音波顕微鏡用のトランスデューサは、高分解能の要求から 200MHz 以上の高い周波数が求められるため、ZnO 圧電薄膜材料を用いたトランスデューサを開発してきた。一般に超音波診断装置（通称エコー）用の超音波トランスデューサには Pb（Zr, Ti）O3 セラミックス（PZT セラミックス）が使用されているが、PZT セラミックスはもろい為、0.1mm より薄い厚さとなる 20MHz を超える高周波振動子を製作することは難しい。別の手法として、樹脂とセラミックスのコンポジット材料を用いた材料開発が試みられているが、その周波数は 50MHz 程度の高周波である。また、PVDF, ZnO の圧電定数 kT は 13%、24%と、PZT セラミックスの 62%と比べ格段にパフォーマンスが悪い材料である。我々は、パルス励起を行なうために、感度の点からパフォーマンスの良い PZT セラミックスを出発原料にして、高周波に対応できる数μm の厚膜を金属板上に成膜する技術を検討していく。この新しい手法を用い、セラミックス粉末からパルス励起でも高感度化を達成できる超音波顕微鏡用トランスデューサの基礎実験を行ない、数 10MHz 以上の超音波顕微鏡用素子を製作する技術を検討した。その他にガスデポジション法を用いた ZnO 高速厚膜成長実験も同時に行なった。

(1)ガスデポジション法

ガスデポジション法を用いた ZnO 高速厚膜成長実験（図 17）を行い、装置の使用時間の短縮から、超音波顕微鏡用トランスデューサのコストダウンを試みた。可能性を探るため 100 サンプルの規模で研究し、ZnO 膜をサファイア基板上に、30μm/h から 100μm/h の成膜速度を達成し、従来のスパッタ法（0.2μm/h）と比べ、150 倍早い成膜手法を確立した。しかし、電気機械結合定数 kT は 24%と PZT セラミックスに比べ小さな値であった。

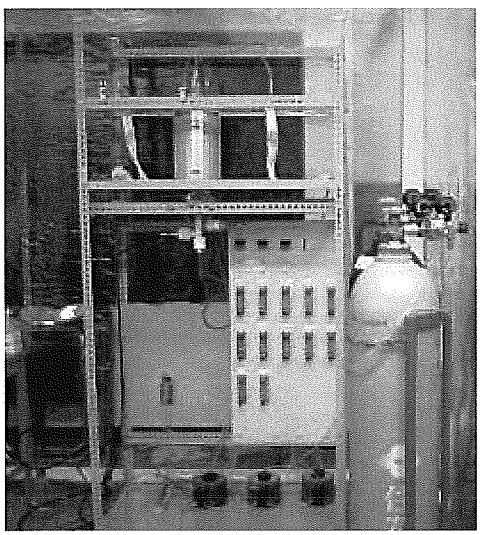

図 17 ZnO 高速製造装置

(2)新しい厚膜製作手法の研究

新しい成膜手法として、セラミックス粉末を用いた厚膜成長テストを行った。可能性を探るため 50 サンプルの規模で PZT セラミックスの成膜実験を行った。その結果、ステンレス基板上に PZT セラミックスを成膜することができた。ステンレス基板上に成膜された PZT セラミックスの膜厚は 50μm で、成膜時間は 15 分間であった（図 18、

図 19)。表面は数μm の平坦さを保っており、条件をコントロールすれば、200μm/h の速度で高速成膜でき、膜厚もコントロール可能であることが分かった（図 20)。

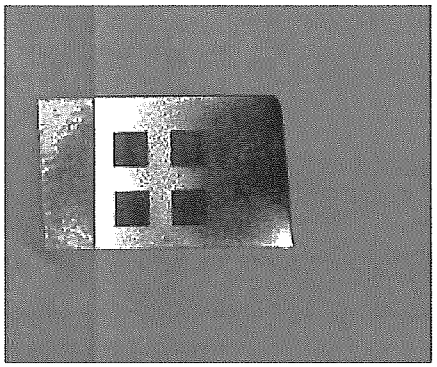

図 18 ステンレス基板上の PZT

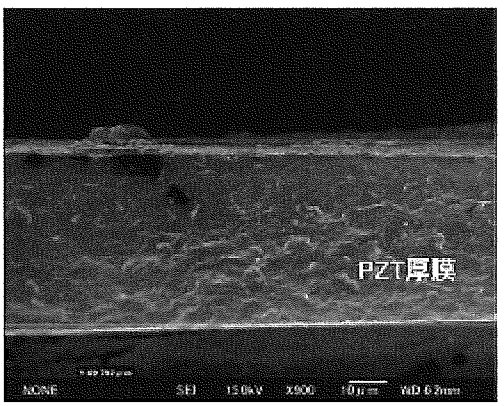

図 19 PZT 厚膜の電子顕微鏡観察

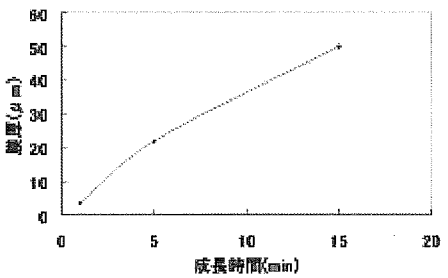

図 20 PZT 厚膜の成膜速度

D. 考 察

厚さ 1mm のステンレス基板上に PZT セラミックスを数 10μm の均一な厚膜を作製するテストは成功した。

しかし、超音波顕微鏡用トランスデューサを考えた場合、ステンレス基板よりガラス基板への成膜の方が水へのマッチングが良い。このため、ガラス基板の上に、電気信号を取り出すための電極を形成し、PZT

厚膜を作製しなければならない。ガラス基板、または、サファイア基板の上で、製膜時、その後の熱処理でも剥がれない丈夫な電極の形成手法、基板にダメージの無い PZT セラミックス成膜条件の研究がひとつのキーテクノロジーとなると考えている。最終的には平成15年度に試作したZnO型トランスデューサと似た形状への成膜も検討していく。

E. 結 論

金電極を蒸着させたサファイアレンズに対して ZnO の単結晶を DC スパッタ装置により生成し、サファイアとの逆面に再度、金電極を蒸着してケーシングし、ケースに入れ配線をして充填を行うことで、振動子の作製を行なった。作成した振動子の特性では受信のピークが 326MHz であり、挿入損失は 48dB であった。

また、新しい成膜手法として、セラミックス粉末を用いた厚膜成長テストを行い、ステンレス基板上に PZT セラミックスを成膜することができた。

F. 健康危険情報

なし

G. 研究発表

1. 論文発表

1) Hozumi N, Kimura A, Terauchi S, Nagao M, Yoshida S, Kobayashi K, Saijo Y. Acoustic Impedance Micro-imaging for Biological Tissue Using a Focused Acoustic Pulse with a Frequency Range up to 100 MHz. *Proc 2005 IEEE International Ultrasonics Symposium*, 170-173, 2005.
2) Saijo Y, Sasaki H, Yambe T, Tanaka M, Hozumi N, Kobayashi K, Okada N. Speed of Sound Microscopy for Biomedical Applications. *Proc 2005 IEEE International Ultrasonics Symposium*, 423-426, 2005.
3) Miyasaka M, Sakai S, Kusaka A, Endo Y, Kobayashi M, Kobayashi K, Hozumi N, Tanino R. Ultrasonic tissue characterization of photodamaged skin by scanning acoustic microscopy. *Tokai J Exp Clin Med.* Vol. 30, No. 4: 217-225, 2005
4) 小林和人. 特集　ディジタル画像計測とパターン認識の技術　第 5 章　新しい組織観察法を提供する新技術　超音波音速顕微鏡の開発と画像処理. Interface, Vol.31, No.3, 93-104, 2005.
5) 小林和人、穂積直裕、西條芳文、大槻茂雄. 生体組織診断のためのパルス励起型音速顕微鏡の開発. 日本音響学会誌　掲載決定

2. 学会発表

1) Hozumi N, Kimura A, Terauchi S, Nagao M, Yoshida S, Kobayashi K, Saijo Y. Acoustic Impedance Micro-imaging for Biological Tissue Using a Focused Acoustic Pulse with a Frequency Range up to 100 MHz. *2005 IEEE International Ultrasonics Symposium*, Sep 19, 2005, Rotterdam, The Netherlamds.
2) Saijo Y, Sasaki H, Yambe T, Tanaka M, Hozumi N, Kobayashi K, Okada N. Speed of Sound Microscopy for Biomedical Applications. *2005 IEEE International Ultrasonics Symposium*, Sep 21, 2005, Rotterdam, The Netherlamds.

H. 知的所有権の取得状況

該当なし

研究成果の刊行に関する一覧表

書籍

著者氏名	論文タイトル名	書籍全体の編集者名	書籍名	出版社名	出版地	出版年	ページ

雑誌

発表者氏名	論文タイトル名	発表誌名	巻名	ページ	出版年
Saijo Y, Sasaki H, Hozumi N, Kobayashi K, Tanaka M, Yambe T	Sound speed scanning acoustic microscopy for biomedical applications.	*Technol Health Care*	Vol. 13, No. 4	261-267	2005
Funamoto K, Hayase T, Saijo Y, Yambe T	Detection and correction of aliasing in ultrasonic measurement of blood flows with Ultrasonic-Measurement-Integrated simulation	*Technol Health Care*	Vol. 13, No. 4	331-344	2005
Funamoto K, Hayase T, Shirai A, Saijo Y, Yambe T	Fundamental study of ultrasonic-measurement-integrated simulation of real blood flow in the aorta.	*Ann Biomed Eng*	Vol. 33, No. 4	415-428	2005
Watanabe S, Suzuki N, Kudo A, Suzuki T, Abe S, Suzuki M, Komatsu S, Saijo Y, Murayama N	Influence of aging on cardiac function examined by echocardiography.	*Tohoku J Exp Med*	Vol. 207, No.1	13-19	2005
Watanabe M, Sekine K, Hori Y, Shiraishi Y, Maeda T, Honma D, Miyata G, Saijo Y, Yambe T	Artificial esophagus with peristaltic movement.	*ASAIO J*	Vol. 51, No.2	158-161	2005

Santos Filho E, Yoshizawa M, Tanaka A, Saijo Y, Iwamoto T.	Moment based texture segmentation of intravascular ultrasound images.	*J Med Ultrasonics*	Vol. 32, No. 3	91-99	2005
Miyasaka M, Sakai S, Kusaka A, Endo Y, Kobayashi M, Kobayashi K, Hozumi N, Tanino R	Ultrasonic tissue characterization of photodamaged skin by scanning acoustic microscopy.	*Tokai J Exp Clin Med*	Vol. 30, No. 4	217-225	2005
Saijo Y, Hozumi N, Kobayashi K, Okada N, Fukuma K, Tanaka N, Sasaki H, Tanaka M, Yambe T	Acoustic microscopy based on frequency domain analysis of a single pulsed wave.	*Proc 6th Asian-Pacific Conference on Medical and Biological Engineering*	N.A	N.A	2005
Saijo Y, Akino Y, Watanabe S, Oba K, Tamamura K, Yamazaki Y, Ishiguro T	Fully-automatic measurement of flow mediated dilatation.	*Proc 6th Asian-Pacific Conference on Medical and Biological Engineering*	N.A	N.A	2005
Saijo Y, Santos Filho E, Yambe T, Tanaka A, Iwamoto T, Yoshizawa M, Akino Y, Hanadate Y	Parametric intravascular ultrasound imaging - Two-dimensional tissue velocity imaging and self-organizing map imaging.	*Proc 8th Sendai Symposium on Ultrasonic Tissue Characterization*	Vol. 1	1-4	2005
Santos Filho E, Saijo Y, Yoshizawa M, Tanaka A	Automatic luminal contour and calcification detection in intravascular ultrasound images.	*Proc 8th Sendai Symposium on Ultrasonic Tissue Characterization*	Vol. 1	5-8	2005
Saijo Y, Sasaki H, Santos Filho E, Yambe T, Tanaka M, Hozumi N, Kobayashi K	Speed-of sound microscopy for biomedical applications.	*Proc 8th Sendai Symposium on Ultrasonic Tissue Characterization*	Vol. 1	26-29	2005

Kimura A, Terauchi S, Murakami Y, Hozumi N, Nagao M, Yoshida S, Kobayashi K, Saijo Y	Image processing for pulse driven biological microscope based on frequency spectrum.	*Proc 8th Sendai Symposium on Ultrasonic Tissue Characterization*	Vol. 1	30-31	2005
Hagiwara Y, Matsumoto F, Chimoto E, Kokubun S, Saijo Y, Sasano Y	Increased sound speed of synovial membrane after immobilization assessed by scanning acoustic microscopy.	*Proc 8th Sendai Symposium on Ultrasonic Tissue Characterization*	Vol. 1	32-35	2005
Sano H, Hattori K, Kokubun S, Saijo Y	Material properties of the rabbit supraspinatus tendon and its insertion - A measurement with the scanning acoustic microscopy.	*Proc 8th Sendai Symposium on Ultrasonic Tissue Characterization*	Vol. 1	36-38	2005
西條芳文	特集　心血管画像診断の新しい展開　超音波顕微鏡.	*循環器科*	Vol. 57, No. 5	440-446	2005
西條芳文	特集　DES 時代の Beyond Angiography　Virtual Histology の基礎.	*Coronary Intervention*	Vol. 2, No. 1	82-87	2005
西條芳文	特集　冠動脈を診る－壁の性状を識る－　Expertise　冠動脈イメージングの新技術　超音波顕微鏡と Intravascular tissue velocity imaging.	*Heart View*	Vol. 10, No. 3	94-98	2006

研究成果の刊行物・別刷

Technology and Health Care 13 (2005) 261–267
IOS Press

Sound speed scanning acoustic microscopy for biomedical applications

Yoshifumi Saijo[a,*], Hidehiko Sasaki[a], Naohiro Hozumi[b], Kazuto Kobayashi[c], Motonao Tanaka[a] and Tomoyuki Yambe[a]
[a]*Department of Medical Engineering and Cardiology, Institute of Development, Aging and Cancer, Tohoku University, Sendai, Japan*
[b]*Department of Electrical and Electronic Engineering, Toyohashi University of Technology, Sendai, Japan*
[c]*Honda Electronics Co. Ltd., Sendai, Japan*

Received 30 August 2004
Revised 27 January 2005

Abstract. Since 1985, we have been developing a scanning acoustic microscope (SAM) system for biomedical use and have been investigating the acoustic properties of various organs and disease states by using this SAM system. In biomedicine, SAM is useful for intraoperative pathological examination, study of low-frequency ultrasonic images, and assessment of biomechanics at a microscopic level. Recently, we have proposed a new concept – acoustic microscopy – using a single pulsed wave instead of continuous waves used in conventional SAM systems. In the present study, we compared two systems by measuring the same biological material. The sound speed image obtained by sound speed microscopy corresponded well to that obtained using a conventional SAM system. Lesions with hyaline degeneration showed a lower sound speed when compared with that of normal myocardium. Frequency domain analysis of amplitude and phase by both methods also showed similar characteristics. Although the data acquisition time of one frame was greater than that in conventional SAM, the total time required for calculation was significantly shorter. The SAM system can be applied to intraoperative pathological examination.

1. Introduction

Since 1985, we have been developing a scanning acoustic microscope (SAM) system for biomedical use and have been investigating the acoustic properties of various organs and disease states by using this SAM system [1–9]. In biomedicine, SAM is useful for intraoperative pathological examination, study of low-frequency ultrasonic images, and assessment of biomechanics at a microscopic level. The originality of the traditional SAM system lies in providing quantitative values of attenuation and sound speed of thin slices of soft tissue. Although the system may be currently in use, it cannot be repaired because it was constructed using precise hand-crafted technologies and analog signal acquisition circuits. In particular, the x-axis scan is driven by a spiral spring technique that originated from the technologies used in the Japanese watch industry.

*Address for correspondence: Yoshifumi Saijo, Affiliation: Department of Medical Engineering and Cardiology, Institute of Development, Aging and Cancer, Tohoku University, 4-1 Seiryomachi, Aoba-ku, Sendai 980-8575, Japan. Tel.: +81 22 717 8517; Fax: 81 22 717 8518; E-mail: saijo@idac.tohoku.ac.jp.

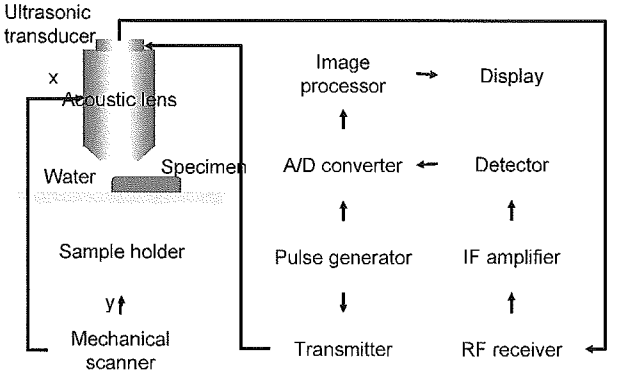

Fig. 1. Block diagram of the scanning acoustic microscope system developed by Tohoku University and Honda Electronics Co. Ltd. in 1985.

Recently, we have proposed a new concept – acoustic microscopy – using a single pulsed wave instead of continuous waves used in conventional SAM systems. In the present study, we compared two systems by measuring the same biological material.

2. Methods

2.1. Tissue preparation

A heterotopic abdominal cardiac transplantation was performed in a mouse. The mouse was not administered any anti-immune drugs. The mouse was killed 7 days after surgery. In order to obtain cross sections of the heart, histological specimens were prepared, and 10 μm and 4 μm thick sections were obtained for scanning acoustic microscopy and Elastica-Masson staining for optical microscopy, respectively. The specimen was ranked AR grade 3 based on the following scale of increasing levels of allograft rejection (AR): AR grade 0 (normal), AR grade 1 (lymphocyte infiltration), AR grade 2 (focal necrosis), AR grade 3 (diffuse necrosis), and AR grade 4 (presence of hemorrhages) as proposed in the Journal of Heart and Lung transplantation.

2.2. Conventional scanning acoustic microscopy

Figure 1 shows a block diagram of the conventional SAM system that operates in the frequency range of 100–200 MHz. The acoustic focusing element comprises a ZnO piezoelectric transducer with a sapphire lens whose aperture half angle is 30°. The lens focuses the acoustic beam with lateral resolution. Its half power width is from approximately 6 μm at 200 MHz to 12 μm at 100 MHz in water at 20°C. Forty continuous ultrasonic pulses were input to the transducer from an analog pulse generator at an arbitrary frequency. The focusing element is mechanically scanned at 60 Hz by using a precise spiral spring in the lateral direction (x) above the specimen. The sampling holder is scanned in the other lateral direction (y) by a stepping motor in 8 s, thus providing two-dimensional scanning. Two-dimensional distribution of amplitude and phase is obtained in a 0.5 mm, 1 mm, or 2 mm field of view. The image processor stored the eleven frames of amplitude images in 10 MHz steps in the range 100 to 200 MHz and 5 phase images in 10 MHz steps in the range 100 to 140 MHz. The thickness of the specimen was determined from the frequency-dependent characteristics of the amplitude and phase of the received signals obtained at the

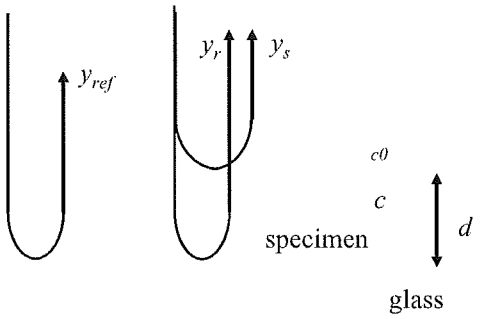

Fig. 2. Schematic illustration of reflections. y_{ref}: reflection from glass, y_r: reflection from the interface between glass and tissue, y_s: reflection from tissue surface.

same position for each of the sixteen frames. The attenuation was then determined from the amplitude and thickness, and the sound speed was determined from the phase shift and thickness.

Figure 2 shows a schematic of pulse propagation in water, tissue, and glass surface. Equation (1) shows the relationship between the frequency, amplitude, and phase due to interference between the reflections from the upper and lower surfaces of the specimen.

$$\begin{aligned} y_r &= y_s + y_b \\ &= e^{-(\alpha + j\frac{2\pi f}{c})d} \\ &= e^{-j\frac{2\pi f}{c}d} \cdot e^{-A_0 f^n d} \end{aligned} \tag{1}$$

where y_r is the received signal, y_s is the signal reflected from the surface of the specimen, y_b is the signal reflected from the interface between the tissue and glass, f is the frequency, c is the sound speed of the specimen, and d is the thickness of the specimen. The thickness was calculated at six regions in an image. The average value of thickness was applied to all pixels for calculation of attenuation and sound speed.

2.3. Sound speed scanning acoustic microscopy

Figure 3 shows a block diagram of sound speed microscopy for biological tissue characterization. A single ultrasound pulse with a pulse width of 5 ns was emitted and received by the same transducer above the specimen. The aperture diameter of the transducer was 1.2 mm, and the focal length was 1.5 mm. The central frequency was 80 MHz, and the pulse repetition rate was 10 kHz. The diameter of the focal spot was estimated to be 20 μm at 80 MHz by taking into account the focal distance and sectional area of the transducer. Distilled water was used as the coupling medium between the transducer and the specimen. The reflections from the tissue surface and those from the interface between the tissue and glass were received by the transducer and were introduced into a digital oscilloscope (Tektronics TDS 5052, USA). The frequency range was 300 MHz, and the sampling rate was 2.5 GS/s. Four values of the time taken for a pulse response at the same point were averaged in the oscilloscope in order to reduce random noise.

The transducer was mounted on an X-Y stage with a microcomputer board that was driven by the computer installed in the digital oscilloscope through RS232C. The X-scan was driven by a linear servo motor, and the Y-scan was driven by a stepping motor. Finally, two-dimensional distributions of ultrasonic intensity, sound speed, and thickness of a specimen measuring 2.4 × 2.4 mm were visualized using 300 × 300 pixels. The total scanning time was 121 s.

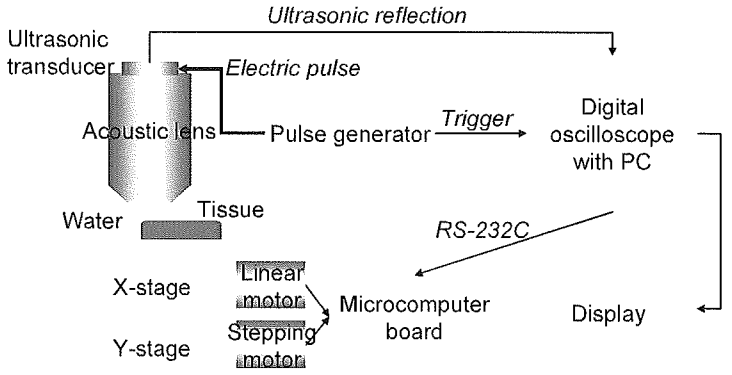

Fig. 3. Block diagram of sound speed scanning acoustic microscopy developed with collaboration between Tohoku University, Toyohashi University of Technology and Honda Electronics Co. Ltd. in 2003.

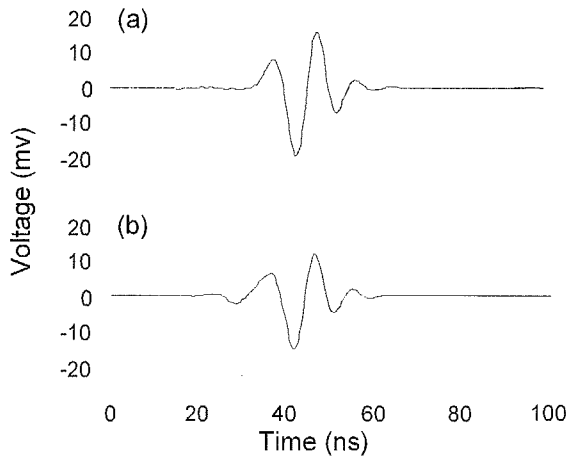

Fig. 4. Reflected waveforms (a) from the glass surface without tissue, and (b) from the tissue area.

2.4. *Signal analysis [10]*

The reflected waveforms are shown in Fig. 4. The waveform at the glass surface without the tissue is shown in (a). This signal was used as a reference waveform. The decline of the glass surface was compensated by measuring three different points in the glass area surrounding the tissue. The waveform from the tissue area is shown in (b). Although the waveform contains two reflections at the surface and at the interface of the tissue and glass, the two components cannot be separated in time domain analysis. Thus, frequency domain analysis was performed by analyzing the interference between the two reflections. Intensity and phase spectra were calculated by Fourier transforming the waveform. The spectra were normalized by the reference waveform. Figure 5 shows the frequency domain analysis of the interfered waveform.

Denoting the minimum point in the intensity spectrum by $f_{\min}$ and the corresponding phase angle by

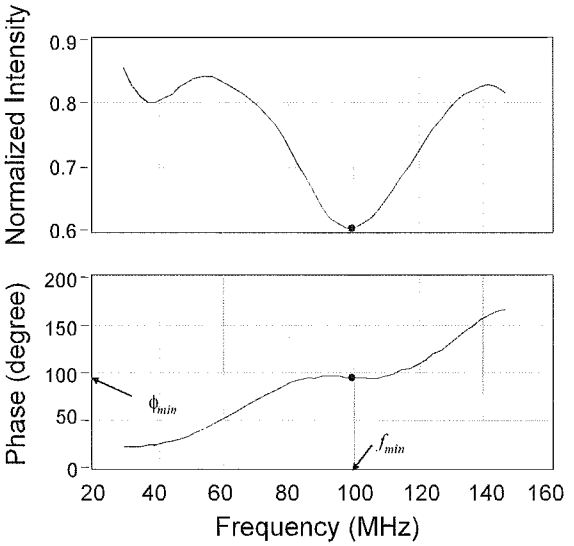

Fig. 5. Frequency domain analysis of interfered waveform. $f_{\min}$: the minimum point in the intensity spectrum, $\phi_{\min}$: corresponding phase angle.

$\phi_{\min}$, the phase difference between the two reflections at the minimum point is $(2n-1)\pi$, which yields

$$2\pi \boldsymbol{f}_{\min} \times \frac{2\boldsymbol{d}}{c_0} = \phi_{\min} + (2\boldsymbol{n}-1)\pi \tag{2}$$

where $\boldsymbol{d}$, c_0, and $\boldsymbol{n}$ are the tissue thickness, sound speed of water, and a non-negative integer, respectively. Denoting the maximum point in the intensity spectrum by $\boldsymbol{f}_{\max}$ and the corresponding phase angle by $\phi_{\max}$, the phase difference at the maximum point is $2n\pi$, which yields

$$2\pi \boldsymbol{f}_{\max} \times \frac{2\boldsymbol{d}}{c_0} = \phi_{\max} + 2\boldsymbol{n}\pi \tag{3}$$

The phase angles $\phi_{\min}$ and $\phi_{\max}$ can be expressed by

$$2\pi \boldsymbol{f}_{\min} \times 2\boldsymbol{d}\left(\frac{1}{c_0} - \frac{1}{c}\right) = \phi_{\min} \tag{4}$$

$$2\pi \boldsymbol{f}_{\max} \times 2\boldsymbol{d}\left(\frac{1}{c_0} - \frac{1}{c}\right) = \phi_{\max} \tag{5}$$

since $\phi_{\min}$ or $\phi_{\max}$ is the phase difference between the wave that travels the distance $2\boldsymbol{d}$ with sound speed c and the wave that travels a corresponding distance with sound speed $\boldsymbol{c}_0$. By solving Eqs (2) and (4),

$$\boldsymbol{d} = \frac{\boldsymbol{c}_0}{4\pi \boldsymbol{f}_{\min}}\{\phi_{\min} + (2\boldsymbol{n}-1)\pi\} \tag{6}$$

is obtained for the minimum point. Solving Eqs (3) and (5) yields

$$\boldsymbol{d} = \frac{\boldsymbol{c}_0}{4\pi \boldsymbol{f}_{\max}}(\phi_{\max} + 2\boldsymbol{n}\pi) \tag{7}$$

for the maximum point. Finally, the sound velocity at each frequency is calculated as

$$c = \left(\frac{1}{c_0} - \frac{\phi_{\min}}{4\pi f_{\min} d} \right) \tag{8}$$

$$c = \left(\frac{1}{c_0} - \frac{\phi_{\max}}{4\pi f_{\max} d} \right) \tag{9}$$

The specimen was first scanned by the conventional SAM, and the obtained image was compared with an optical microscope image of the neighboring section. The same specimen was then scanned with sound speed acoustic microscopy in order to visualize the same area. These two types of images were broadly compared and the frequency-dependent characteristics of the amplitude and phase of a region of interest were also compared.

3. Results

Figure 6 shows (a) optical microscopic image, (b) attenuation image from conventional SAM, (c) sound speed image from conventional SAM, (d) intensity image from sound speed SAM, and (e) sound speed image from sound speed SAM of a rat cardiac allograft model. Figure 6(a) shows that the left part (inner part) is necrotic tissue with hyaline degeneration, and the right part (outer part) is normal myocardium. In Fig. 6(b), the attenuation was 0.8 dB/mm/MHz in the necrotic tissue and 1.2 dB/mm/MHz in the normal myocardium. In Fig. 6(c), the sound speed was 1580 m/s in the necrotic tissue and 1610 m/s in the normal myocardium. An intensity image was generated by two-dimensional distribution of a peak signal amplitude. As a result, the information of the image was different from that of the attenuation image obtained using conventional SAM. In Fig. 6(e), the sound speed was 1580 m/s in the necrotic tissue and 1610 m/s in the normal myocardium.

4. Discussion

In the present study, the entire image of a particular portion obtained using a conventional acoustic microscope was compared with a corresponding image of the same portion obtained using a sound speed microscope. The frequency dependency of amplitude and phase at the same ROI in a specimen was also compared by the frequency variation and Fourier transform methods.

The sound speed image obtained by sound speed microscopy corresponded well to that obtained by conventional SAM. Lesions with hyaline degeneration showed lower sound speed when compared with that of normal myocardium. Frequency domain analysis of amplitude and phase by both methods also showed similar characteristics. The data acquisition time of a frame was 8 s in conventional SAM and 121 s in sound speed microscopy. However, more than ten hours were required to calculate the quantitative values of attenuation and sound speed of an image by conventional SAM, while the same calculation was performed in less than a minute by sound speed microscopy. Conventional SAM requires a skilled operator, for example, to correct the tilting of specimens. The tilt is automatically corrected in sound speed microscopy, and the interface is user-friendly and can be easily operated by medical and pathological researchers.

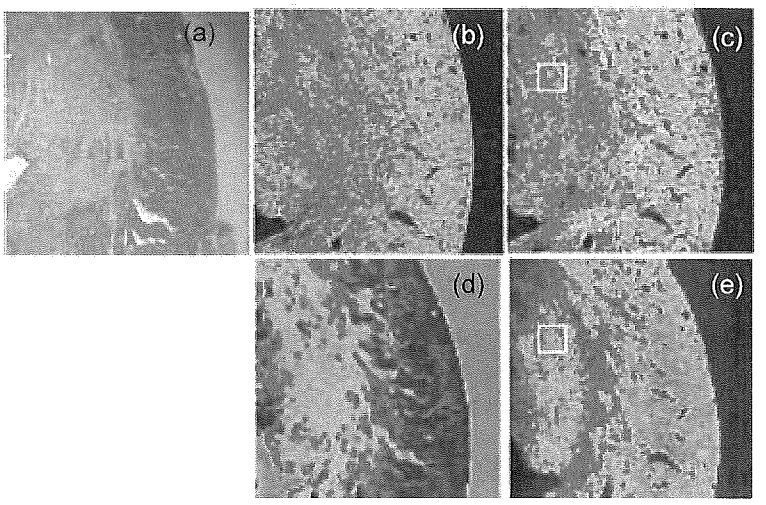

Fig. 6. (a) Optical microscopic image, (b) attenuation image of conventional SAM, (c) sound speed image of conventional SAM, (d) intensity image of sound speed SAM, and (e) sound speed image of sound speed SAM, of a rat cardiac allograft model. ROIs are shown in Fig. 6(c) and (e).

5. Conclusions

An acoustic microscope system that can measure the sound speed of thin slices of biological material was developed. It was a unique acoustic microscope because it used a single pulse and the Fourier transform to calculate the sound speed at all measuring points. Although the data acquisition time of a frame was greater than that in conventional SAM, the total time required for calculation was significantly shorter. The acoustic microscope system can be applied to intraoperative pathological examination.

References

[1] Y. Saijo, M. Tanaka, H. Okawai and F. Dunn, The ultrasonic properties of gastric cancer tissues obtained with a scanning acoustic microscope system, *Ultrasound Med Biol* **17** (1991), 709–714.
[2] H. Sasaki, M. Tanaka, Y. Saijo, H. Okawai, Y. Terasawa, S. Nitta and K. Suzuki, Ultrasonic tissue characterization of renal cell carcinoma tissue, *Nephron* **74** (1996), 125–130.
[3] Y. Saijo, M. Tanaka, H. Okawai, H. Sasaki, S. Nitta and F. Dunn, Ultrasonic tissue characterization of infarcted myocardium by scanning acoustic microscopy, *Ultrasound Med Biol* **23** (1997), 77–85.
[4] Y. Saijo, H. Sasaki, H. Okawai, S. Nitta and M. Tanaka, Acoustic properties of atherosclerosis of human aorta obtained with high-frequency ultrasound, *Ultrasound Med Biol* **24** (1998), 1061–1064.
[5] Y. Saijo, H. Sasaki, M. Sato, S. Nitta and M. Tanaka, Visualization of human umbilical vein endothelial cells by acoustic microscopy, *Ultrasonics* **38** (2000), 396–399.
[6] Y. Saijo, T. Ohashi, H. Sasaki, M. Sato, C.S. Jorgensen and S. Nitta, Application of scanning acoustic microscopy for assessing stress distribution in atherosclerotic plaque, *Ann Biomed Eng* **29** (2001), 1048–1053.
[7] H. Sasaki, Y. Saijo, M. Tanaka and S. Nitta, Influence of tissue preparation on the acoustic properties of tissue sections at high frequencies, *Ultrasound Med Biol* **29** (2003), 1367–1372.
[8] Y. Saijo, T. Miyakawa, H. Sasaki, M. Tanaka and S. Nitta, Acoustic properties of aortic aneurysm obtained with scanning acoustic microscopy, *Ultrasonics* **42** (2004), 695–698.
[9] H. Sano, Y. Saijo and S. Kokubun, Material properties of the supraspinatus tendon at its insertion – A measurement with the scanning acoustic microscopy, *J Musculoskeletal Res* **8** (2004), 29–34.
[10] N. Hozumi, R. Yamashita, C.K. Lee, M. Nagao, K. Kobayashi, Y. Saijo, M. Tanaka, N. Tanaka and S. Ohtsuki, Time-frequency analysis for pulse driven ultrasonic microscopy for biological tissue characterization, *Ultrasonics* **42** (2004), 717–722.

Technology and Health Care 13 (2005) 331–344
IOS Press

Detection and correction of aliasing in ultrasonic measurement of blood flows with Ultrasonic-Measurement-Integrated simulation

Kenichi Funamoto[a], Toshiyuki Hayase[b,*], Yoshifumi Saijo[c] and Tomoyuki Yambe[c]
[a]*Graduate School of Engineering, Tohoku University, Sendai, Japan*
[b]*Institute of Fluid Science, Tohoku University, Sendai, Japan*
[c]*Institute of Development, Aging and Cancer, Tohoku University, Sendai, Japan*

Abstract. Detailed information of real blood flows is essential to develop an accurate diagnosis or treatment for serious circulatory diseases such as aortic aneurysms. *Ultrasonic-Measurement-Integrated (UMI) simulation*, in which feedback signals from the ultrasonic measurement make the simulation converge to the real blood flow, is a key to solving this problem. However, aliasing in the ultrasonic blood velocity measurement causes UMI simulation to converge to an erroneous result. In this paper, we have investigated the detection and the correction of aliasing in UMI simulation. The artificial force in the feedback of UMI simulation can be used as an index to detect the aliasing. We have proposed two ways for the correction of the aliasing. Correction A, in which measurement velocity is replaced with the computational one at the monitoring point where the aliasing is detected, substantially improves the accuracy of UMI simulation. Correction B, in which measurement velocity is replaced with an estimated Doppler velocity, can provide exactly the same result as that of UMI simulation using the nonaliased standard solution. Although correction B gives the most accurate result, correction A seems more robust and, therefore, a beneficial choice considering the other artifacts in the measurement.

1. Introduction

Recently, many researches have focused on the relationship between circulatory diseases and hemodynamics, such as the development, progress, and rupture of aneurysm and wall shear stress [1–4]. For elucidation, the numerical simulation of blood flow has been performed extensively using realistic vessel geometries obtained by medical imaging techniques such as magnetic resonance imaging (MRI) or computed tomography (CT) [5–9]. These studies have provided many insights into the relationship. However, it is difficult for ordinary numerical simulations to exactly reproduce the real blood flow because of an inherent problem of specification of the boundary conditions as well as problem in modeling of complex blood flow problems [6].

For the measurement of blood flows, ultrasonic diagnostic equipment is the most widely used for the diagnosis of blood vessel diseases among all imaging technologies. It can non-invasively provide real-time images of the blood flow and vessel configuration *in vivo* by color Doppler ultrasonography [10].

*Address for correspondence: Dr. T. Hayase, Institute of Fluid Science, Tohoku University, 2-1-1 Katahira, Aoba-ku, Sendai, Miyagi 980-8577, Japan. Tel./Fax: +81 22 217 5253; E-mail: hayase@ifs.tohoku.ac.jp.

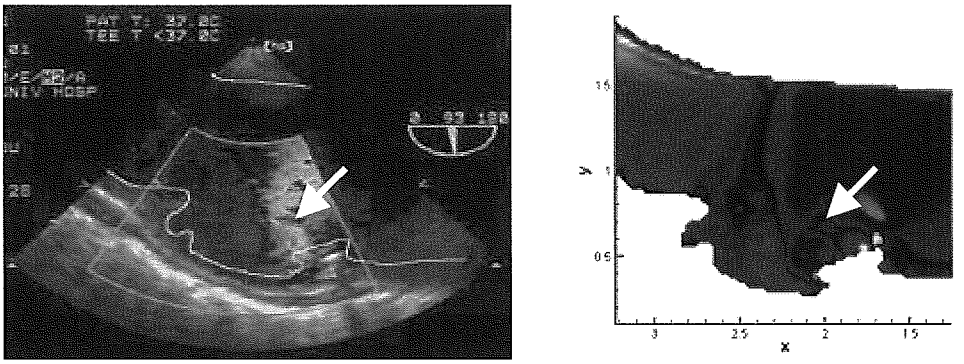

(a) (b)

Fig. 1. (a) Color Doppler image around a thoracic aneurysm (Center frequency f_C: 4.4 MHz, Pulse repetition frequency f_R: 4 kHz) and (b) that of UMI simulation.

However, the blood flow measurement is limited to the velocity component in the ultrasonic beam direction or Doppler velocity, since it converts the Doppler shift frequency to the velocity. The blood flow is visualized by color Doppler image which displays colors of graduated intensity, blue for flow away from the probe and red for flow approaching the probe for instance, superimposing on the B-mode image, which shows the configuration of the blood vessel wall with gray scale, as shown in Fig. 1(a). Unfortunately, it is difficult to recognize the exact three-dimensional structure of the blood flow from the color Doppler image.

In order to solve those problems both in numerical simulation and in measurement as described above, Ultrasonic-Measurement-Integrated (UMI) simulation has been proposed by the present authors [11]. It integrates the color Doppler ultrasonography and numerical simulation and makes it possible to reproduce the blood flow on a computer. During the computational process, feedback signals are generated from the difference between the output signals of the measurement and those of the computation, and are added to the simulation to compensate for the difference. In the former study [11], the characteristics of UMI simulation are studied in a two-dimensional model problem, showing that the result of UMI simulation in feedback domain rapidly converges to the standard solution, even with usually incorrect upstream boundary condition. We also carried out UMI simulation with feedback from real color Doppler measurement and showed good agreement with measurement. In that study, it is observed that UMI simulation follows the measurement data even if it includes the aliasing as shown with white arrow in Fig. 1(b). In fact, the reproduction of aliasing is not desirable since the aliasing region originally shows incorrect data.

In the color Doppler ultrasonography, aliasing occurs in the region where Doppler velocity exceeds the limitation of the measurable velocity. As a result, aliasing region is displayed with incorrect color in the color Doppler image. The elimination of the aliasing is a serious issue for accurate quantification of regurgitation of heart valves in the cardiovascular diagnosis and many methods have been proposed for this problem [12–14]. Fan et al. [13] proposed a new technology termed Quantitative Un-Aliased Speed Algorithm Recognition (Quasar), which employs two color Doppler imaging with two different ultrasound frequencies simultaneously and compute a new operating frequency based on the difference between the two phase shifts for each frequency. Though it allows the measurement of high blood flow velocities accurately during transesophageal color Doppler ultrasonography, it cannot follow the disturbed flow. Stewart [14] performed iterative curve fitting of the jet including the aliasing to a

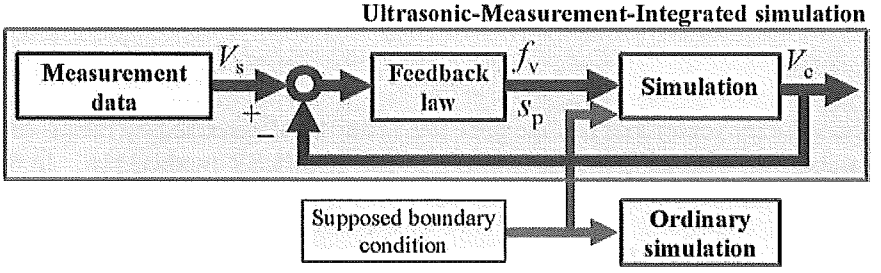

Fig. 2. Block diagram of Ultrasonic-Measurement-Integrated simulation.

mathematical model derived from the jet theory, and distinguished the nonaliased velocities from the aliased ones in steady trial. However, it is difficult to construct the mathematical model when the geometry is complicated or the flow is disturbed.

In this paper, the detection and the correction of the aliasing in UMI simulation are proposed. Magnitude of the feedback in UMI simulation is used as index in determining the aliasing. Two methods are proposed for correction of aliasing. Validation of the proposed methods is examined with a simple two-dimensional model problem for blood flow in an aorta with an aneurysm. A standard solution is first defined as a model of real flow. Aliasing is introduced to the standard solution. The UMI simulation is carried out with the aliased standard solution applying two correction methods after detection of aliasing. For the verification of the effectiveness by the presented algorithms in UMI simulation, UMI simulation without correction, the ordinary simulation and UMI simulation with nonaliased standard solution are also performed.

2. Method to correct aliasing in UMI simulation

2.1. UMI simulation

Ultrasonic-Measurement-Integrated (UMI) simulation is a kind of flow observer to reproduce the real blood flow numerically [15]. The UMI simulation consists of numerical simulation and measurement of blood flow with color Doppler ultrasonography as shown in Fig. 2. During the computational process, the difference between color Doppler images obtained by measurement and simulation is fed back to the numerical simulation. The UMI simulation allows not only reconstruction of the color Doppler image but also the determination of the velocity vectors and the pressure distribution in detail. The following is a brief explanation of this methodology in 2-dimensional formulation. Detailed description is given in another article [11].

As described above, measurement data is obtained by the color Doppler ultrasonography. It can provide real-time images of the anatomy and the blood flow structure simultaneously. The configuration of the blood vessel wall *in vivo* is reconstructed as a B-mode image from time delays and magnitudes of the ultrasonic echo. In addition to that, the blood velocity component in the ultrasonic beam direction, namely the Doppler velocity, is measured by the Doppler shift frequency. For the visualization of the blood flow, the frequency shifts are converted to colors of graduated intensity as shown in Fig. 1(a).

In the numerical simulation, the governing equations are the Navier-Stokes equations for incompressible and viscous fluid flow,

$$\frac{\partial \mathbf{u}}{\partial t} = -(\mathbf{u} \cdot \text{grad})\mathbf{u} + \frac{1}{Re}\nabla^2\mathbf{u} - \text{grad}p, \tag{1}$$

and the equation of continuity,

$$\mathrm{div}\mathbf{u} = 0, \tag{2}$$

where $\mathbf{u} = (u, v)$ is the velocity vector and p is the pressure. They are discretized by means of the finite volume method and are solved with an algorithm similar to the SIMPLER method [16]. In SIMPLER method, x-directional momentum equation is expressed as

$$u_i = (\Sigma B_j u_j + S_i) / B_i + d_i(p_i - p_{i-1}), \tag{3}$$

where $(\Sigma B_j u_j)$ means the summation of the four values circumfusing u_i. By substituting Eq. (3) and similar equations for y-directional momentum to the integrated form of the equation of continuity, the pressure equation is obtained as

$$a_i p_i = \Sigma a_j p_j + s_{pi}, \tag{4}$$

where $(\Sigma a_j p_j)$ means the summation of the values at four adjacent nodes. The notations of the parameters in Eqs (3) and (4), as well as supplementary pressure correction equations and velocity correction procedure in SIMPLER method are explained in a reference [17].

In order to compensate for the difference between the computation and the measurement, feedback signals are applied to the governing equations in the form of source terms. The feedback algorithm consists of feedback to the velocity and pressure fields as follows. As a feedback signal, the artificial force f_v proportional to the difference between Doppler velocities of the measurement and the simulation is applied to the Navier-Stokes equations in the direction of the ultrasonic beam. The force f_v is calculated by the following equation:

$$f_v = -K_v \rho (V_c - V_s) u'_{\max} \Delta S, \tag{5}$$

where K_v is the feedback gain (nondimensional), $u'_{\max}$ is the maximum average flow velocity of the blood flow at the upstream boundary, and ΔS is an interfacial area of the control volume. Here, the artificial force f_v accelerates the fluid to reduce the error in velocity and increases the pressure of the control volume through the pressure Eq. (4). Hence, the other additional feedback signal s_p is introduced to the pressure equation as the source term to counteract the effect of artificial force f_v.

$$s_p = -K_p \rho (V_c - V_s) \Delta S, \tag{6}$$

where K_p is the feedback gain for the pressure (nondimensional).

The calculation of the feedback signal is illustrated in Fig. 3. The purpose of the feedback is to force the velocity $\mathbf{u}_c$ obtained by numerical simulation to converge to the real flow velocity $\mathbf{u}_s$ obtained with ultrasonic diagnostic equipment. The Doppler velocities of the numerical simulation and the measurement, V_c and V_s, are the projection of $\mathbf{u}_c$ and $\mathbf{u}_s$ in the ultrasonic beam direction (a chain line in Fig. 3), respectively. If the computational result V_c is smaller than V_s, the artificial force f_v has a positive value and accelerates the fluid in the ultrasonic beam direction in UMI simulation to reduce the error. The force f_v is decomposed to the x-directional component f_{vx} and the y-directional component f_{vy}, which are added to the control volumes of $u(i, j)$ and $v(i, j)$ in the Navier-Stokes equation, respectively.

For the evaluation of UMI simulation, we define the average error norms $\bar{e}_N$ for an arbitrary variable a, which is the velocity component u, v, V, the velocity vector $\mathbf{u}$ or the pressure p as follows:

$$\bar{e}_N(a) = \frac{1}{N} \sum_n \frac{1}{a_{\max} T} \int_T |a_{cn}(t) - a_{sn}(t)| dt, \tag{7}$$

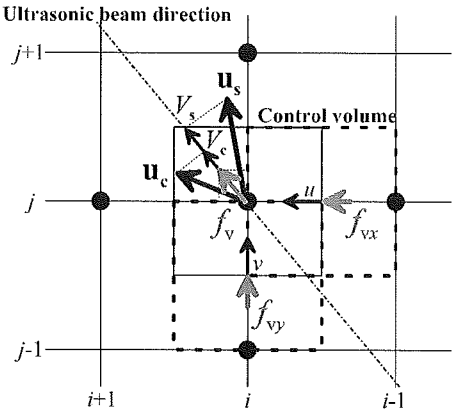

Fig. 3. Computational grid and definition of calculation of feedback signal.

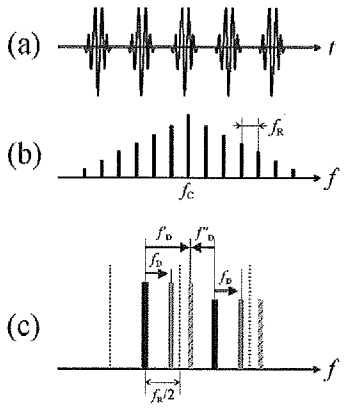

Fig. 4. Schematic diagram of (a) repeated pulse of ultrasound, (b) power spectrum, and (c) Doppler shift.

where N is the total number of the monitoring points, T is the characteristic time, $|\cdot|$ is the absolute value for scalar variables or l_1 norm $|u| + |v|$ for the velocity vector $\mathbf{u}$, $a_{\max}$ is the characteristic value for normalization: $a_{\max} = u'_{\max}$ for velocity or $a_{\max} = \rho u'^2_{\max}$ for pressure. Subscript cn corresponds to UMI simulation, and sn to the measurement, respectively. In the subscripts "cn" and "sn", n is the index of the grid point.

The UMI simulation is specified by the combination of gains (K_v, K_p). Note that the special case with $K_v = K_p = 0$ corresponds to the ordinary simulation without feedback. The values of the gains (K_v, K_p) are determined so that the average error norms $\bar{e}_N(a)$ of some specified variables takes the minimum value over a number of trial computations. The improvement of the computational accuracy by UMI simulation is also evaluated using $\bar{e}_N(a)$ of some specific variables.

2.2. *Correction of aliasing*

Aliasing is a serious error in Doppler measurement resulting in an incorrect magnitude and direction of the velocity. Figure 4 explains the cause of the aliasing. Repeated pulses of ultrasound are emitted from the probe as shown in Fig. 4(a). This ultrasound has a power spectrum with center frequency f_C and pulse repetition frequency interval f_R as shown in Fig. 4(b). In the Doppler velocity measurement,

the Doppler velocity is calculated from the Doppler shift frequency f_D as shown in Fig. 4(c). In case that the Doppler shift frequency f'_D exceeds one half the pulse repetition frequency ($f_R/2$), it is regarded as the Doppler shift from the adjacent frequency (f''_D) and therefore, it leads to the Doppler velocity with incorrect magnitude and direction. Therefore, the measurable Doppler velocity V is expressed as

$$V_{\min} \leqslant V \leqslant V_{\max}, \tag{8}$$

where $V_{\max}$ and $V_{\min}$ are the positive and negative threshold values of measurable Doppler velocity, respectively, and those are determined according to the pulse repetition frequency f_R as shown in Eq. (9).

$$\begin{cases} V_{\max} = \dfrac{cf_R}{4f_C \cos\theta} \\ V_{\min} = -\dfrac{cf_R}{4f_C \cos\theta} \end{cases}, \tag{9}$$

where c is the acoustic velocity and θ is an irradiation angle of ultrasound to the blood flow. In the case that V is larger than $V_{\max}$, the Doppler velocity is regarded as $V_{\min} + (V - V_{\max})$ with the opposite direction. In the case that V is smaller than $V_{\min}$, a similar occurs.

In the former study [11], it was observed that the intensity of the feedback signal $|f_v|$ becomes very large in the region where the aliasing occurs. Here, we use the feedback signal f_v for the detection and the correction of the aliasing. In case that the artificial force f_v calculated by Eq. (5) at a monitoring point is in a normal range,

$$f_{\min} \leqslant f_v \leqslant f_{\max}, \tag{10}$$

where $f_{\min} = K_v \rho V_{\min} u'_{\max} \Delta S$ and $f_{\max} = K_v \rho V_{\max} u'_{\max} \Delta S$, f_v is used for the feedback in UMI simulation with no corrections. In contrast, if f_v is outside the normal range, $f_v < f_{\min}$ or $f_{\max} < f_v$, it is regarded as an unnatural force in the opposite direction due to the aliasing of measured Doppler velocity. In this case, we introduce two ways of correcting the measured Doppler velocity V_s in the feedback in Eqs (5) and (6) as follows.

Correction A: *The measured Doppler velocity is replaced with calculated value as*

$$V_s = V_c. \tag{11}$$

Correction B: *The measured Doppler velocity is replaced with the estimated Doppler velocity considering the effect of the aliasing as*

$$V_s = V_e, \tag{12}$$

where

$$V_e = \begin{cases} V_{\max} - (V_{\min} - V_s) \ (f_v < f_{\min} < 0 \\ V_{\min} - (V_{\max} - V_s) \ (0 < f_{\max} < f_v) \end{cases}. \tag{13}$$

For example, in case that the f_v is smaller than the negative threshold value $f_{\min}$, the Doppler velocity V_s is thought to take the incorrect negative value because of aliasing. We convert the velocity to the positive value by Eq. (13), and apply the feedback signal there using the recalculated positive artificial force f_v.